Journal of Alloys and Compounds 506 (2010) 468–474

Contents lists available at ScienceDirect

Journal of Alloys and Compounds

journal homepage: www.elsevier.com/locate/jallcom

Effect of Y on microstructure and mechanical properties of duplex Mg–7Li alloys

Hanwu Dong[a,b], Lidong Wang[a], Yaoming Wu[a], Limin Wang[a,*]

[a] State Key Laboratory of Rare Earth Resource Utilization, Changchun Institute of Applied Chemistry, CAS, Changchun 130022, China
[b] Graduate University of Chinese Academy of Sciences, Beijing 100049, China

ARTICLE INFO

Article history:
Received 7 December 2009
Received in revised form 7 July 2010
Accepted 7 July 2010
Available online 15 July 2010

Keywords:
Mg–Li alloy
Yttrium
Precipitate phase
Mechanical property

ABSTRACT

Mg–7Li–*x*Y (*x* = 0–7 wt.%) alloys were prepared by permanent mould casting method, and the microstructure and mechanical properties of the alloys were investigated. The results show that α-Mg and β-Li phases exist in all alloys. The Y-enriched α-Mg phase distributes along the edge of α-Mg phase and in the β matrix of *x* = 1–7 alloys, and $Mg_{24}Y_5$ mainly disperses in the β matrix of *x* = 3–7 alloys. The strength of the alloy is enhanced by adding Y element, and the elongation is improved with the Y content no more than 3 wt.%. The as-cast Mg–7Li–3Y alloy exhibits an optimum combination of mechanical properties with the ultimate tensile strength, yield strength and elongation of 160 MPa, 144 MPa and 22%, respectively. After solutionized at 400 °C for 3 h with a subsequent aging at 100 °C, Mg–7Li–7Y alloy exhibits high ultimate tensile strength and yield strength, which are improved to 120% and 152% compared with those of the as-cast Mg–7Li alloy, respectively.

1. Introduction

Mg alloys have drawn increasing attentions in recent years. However, as most Mg alloys possess a hexagonal-closed-packed (HCP, α phase) crystalline structure and a high axial ratio (*c*/*a*) of 1.6236, their plastic processing ability is poor at ambient temperature. This consequently hinders the widespread use of Mg alloys in many application fields. It has been reported that the addition of Li element could decrease the *c*/*a* ratio of hexagonal Mg lattice and even change the crystalline structure of Mg alloys [1]. When Li content exceeds 5.3 wt.%, a Li-based body-centered-cubic (BCC, β phase) structure will be introduced to hexagonal magnesium, which results in (α + β) duplex phases in Mg–Li-based alloys [2].

Mg–Li-based alloys are the lightest metallic structural materials. They possess many special properties such as high specific strength and rigidity, good ductility and good cryogenic properties. These properties enable Mg–Li alloys to be used once as armor materials in military and secondary or non-structural materials in aerospace area [3], and Mg–Li alloys are still drawing experimental and academic interests nowadays [4–6]. Nevertheless, the strength of Mg–Li binary alloys is very low [7]. Alloying elements, such as aluminum, zinc, silver, silicon, cadmium, and rare earth (RE) elements, are introduced to improve the mechanical properties of Mg–Li binary alloys. Among alloying elements, RE elements are effective in improving mechanical properties of Mg–Li-based alloys [8–11]. The RE element of Y was applied to develop Mg–Li–Y ternary alloys by many researchers. However, these researches are concentrated only on Y content of 1 wt.%, 6 wt.% and 8 wt.% with Li content of 8–9 wt.% [12–16]. This work seeks to study the effects of Y content, from 1 wt.% to 7 wt.%, on microstructure and mechanical properties of the duplex Mg–7Li alloys.

2. Experimental procedures

Mg–7Li–*x*Y (*x* = 0 wt.%, 1 wt.%, 3 wt.%, 5 wt.%, and 7 wt.%) alloys were prepared from commercial pure Mg (99.8 wt.%), pure Li (99.9 wt.%), and Mg–19.3 wt.% Y master alloy. The alloys were melted at 750 °C in a mild steel crucible and a mixture flux of LiCl–KCl was used to keep the melts away from the air. After Mg and Mg–Y master alloy were melted, Li was added by an inverted low-carbon steel cup. The melts were kept at 730 °C for 10 min, and then cast into a permanent metal mould preheated to 200 °C with the size of the ingots of 100 mm × 42 mm × 14 mm. Then the ingots were machined to 70 mm × 34 mm × 10 mm. The alloy samples were cut down from the machined ingots and the examinations were carried out. The specimens for heat treatment were wrapped in Al foil and buried in graphite powder. The Y-containing alloys were solutionized for 3 h at 375 °C, 400 °C, 425 °C and 450 °C. Subsequent aging treatment was performed at 100 °C for Mg–7Li–1Y and Mg–7Li–7Y alloys. All heat-treated samples were quenched in room temperature water. The microstructure and mechanical properties were examined. The specimens for tensile tests are dumbbell test pieces with the gauge size of 13 mm × 5 mm × 2 mm.

Chemical composition of the studied alloys was determined by inductively coupled plasma-atomic emission spectrometry (ICP-AES). After etched by nitric acid ethanol solution (4 ml nitric acid, 108 ml ethanol), the microstructure was evaluated by optical microscopy and scanning electron microscopy (SEM) equipped with energy dispersive spectrometer (EDS), backscattered electron (BSE) and electron probe micro-analysis (EPMA) patterns. X-ray diffraction (XRD) analysis was carried out to determine the phases in the alloys. The Vickers hardness (HV) and Brinell hardness (HB) were also tested. The test loads and application times were 25 g and 15 s for HV, and 15.625 kg and 15 s for HB, respectively. The HV of α and β phases in all as-cast alloys was also examined with the load of 10 g and application time of 15 s. Tensile tests were performed at room temperature with an initial rate of 3.3×10^{-4} s^{-1}.

* Corresponding author. Tel.: +86 431 85262447; fax: +86 431 85262447.
E-mail address: lmwang@ciac.jl.cn (L. Wang).

0925-8388/$ – see front matter © 2010 Elsevier B.V. All rights reserved.
doi:10.1016/j.jallcom.2010.07.032

Table 1
Nominal composition and measured composition of the alloys (wt.%) determined by ICP-AES.

Nominal composition	Mg–7Li	Mg–7Li–1Y	Mg–7Li–3Y	Mg–7Li–5Y	Mg–7Li–7Y
Li	7.27	6.50	7.40	7.76	6.90
Y	–	1.17	3.16	4.57	6.89
Mg	Balance	Balance	Balance	Balance	Balance

3. Results and discussion

3.1. Microstructure of as-cast alloys

The chemical compositions of the studied alloys are listed in Table 1. The actual contents of Li and Y are near to the nominal compositions. Fig. 1 illustrates the XRD patterns of the as-cast Mg–7Li–(0–7)Y alloys. Both α-Mg and β-Li phases exist in all alloys. This situation suggests that all Mg–7Li–(0–7)Y alloys are Mg–Li dual-phase alloys. Additionally, $Mg_{24}Y_5$ is detected in Mg–7Li–5Y and Mg–7Li–7Y alloys.

Fig. 2 demonstrates the EPMA mapping of Mg element in Mg–7Li–1Y alloy. The needle-like gray zones are richer in Mg element than the dark background areas. In duplex Mg–Li alloys, the Mg fraction of Mg-based phase is believed to be higher than that of Li-based phase. It is concluded that the need-like and dark zones are α-Mg and β-Li phase, respectively. This is consistent with the results reported by Furui et al. [17].

The optical microstructures of Mg–7Li–(0–7)Y alloys are shown in Fig. 3. In Mg–7Li alloy, the sections of α-Mg grains are mainly petal-like with the average size of about 100 μm and clearance width of 2–8 μm. The grain size of α-Mg phase decreases with the increasing Y content. The sections of α-Mg grains in Mg–7Li–1Y alloy are needle-like, and round-headed sections of α-Mg grains with a size of 10–30 μm are observed in Mg–7Li–(3–7)Y alloys. The grain boundary phase begins to appear in Mg–7Li–3Y alloy and becomes net-like in Mg–7Li–7Y alloy. There are a large amount of small black spots in both α-Mg and β-Li phases of Mg–7Li–7Y alloy, which makes it difficult to distinguish these two phases from each other in low magnification. These spots appear to be precipitates.

SEM is used to probe the microstructure and confirms the phase composition of the investigated alloys. Fig. 4 shows the SEM images of Mg–7Li–(0–7)Y alloys. It is clearly observed that α-Mg phases in these alloys are separated from each other by β-Li phases. Mg–7Li alloy consists of α-Mg and β-Li phases. By adding Y element, a great

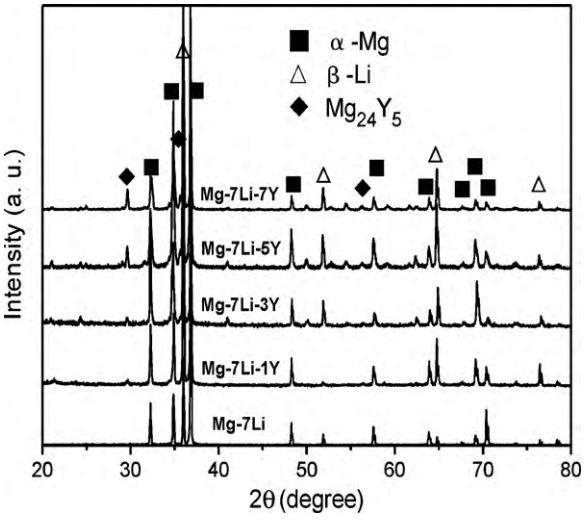

Fig. 1. XRD patterns of the as-cast Mg–7Li–(0–7)Y alloys.

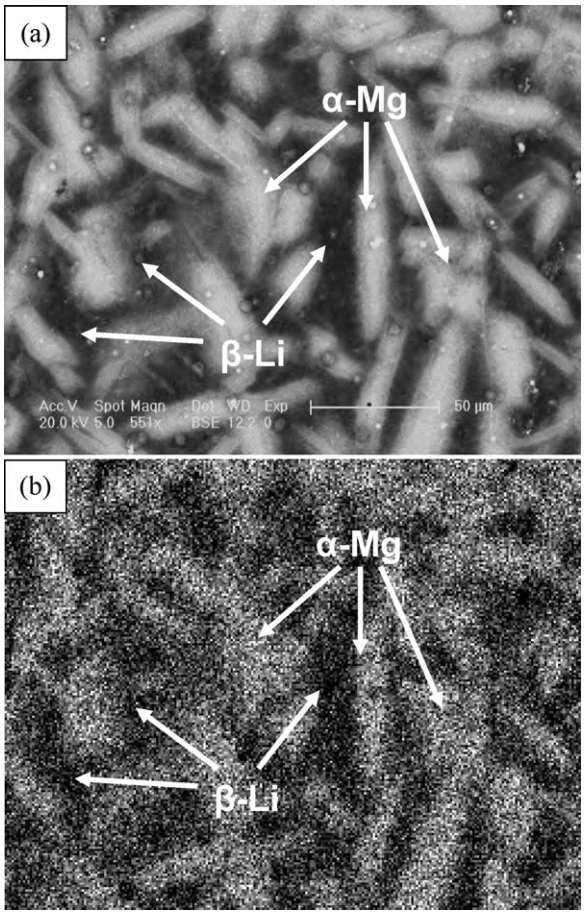

Fig. 2. An SEM image of the as-cast Mg–7Li–1Y alloy (a) and the corresponding EPMA mapping of Mg (b).

number of very finer particles (marked as A) are formed and distributed in the β-Li phase and along the boundaries of α-Mg and β-Li phases, as seen in Fig. 4(b)–(e). Bulky lamellar phase (marked as B) is observed in Fig. 4(c)–(e), and its volume fraction rises when increasing Y content. Besides, some white round dots (labeled as C) are detected in Fig. 4(b).

The compositions of these phases are determined by EDS and the results are listed in Table 2. Since Li element cannot be detected by EDS, the Li content is omitted in this table. The Mg:Y weight ratio of the finer particles is very close to that of the maximal solid solubility of Y in Mg (Mg:Y = 87.44:12.56, in weight) [18]. It was believed that the α-Mg phase precipitates in the β matrix due to the decrease of Mg solubility as the temperature decreases [19]. Accordingly, these particles are concluded to be Y-enriched α-Mg phase. In Fig. 3(f), they are recognized as the small black dots in both α and β phases of Mg–7Li–7Y alloy. The composition of the bulky lamellar phase is near to the eutectic composition of Mg–Y binary system with the Y fraction of 26.3 wt.% [18]. Hence, they are concluded to be the eutecticum of $Mg_{24}Y_5$ and the α-Mg solution with the maximal

Table 2
The compositions determined by EDS of the phases in the as-cast alloys: the Y-enriched α-Mg phase (a), eutecticum phase (b), white round dots (c) and β-Li matrix (d) (Li content not included).

	(a)		(b)		(c)		(d)	
	wt.%	at.%	wt.%	at.%	wt.%	at.%	wt.%	at.%
Mg	88.58	96.60	75.23	91.74	37.77	61.60	99.61	99.89
Y	11.42	3.40	24.77	8.26	56.99	25.41	0.39	0.11
O	–	–	–	–	5.24	12.99	–	–

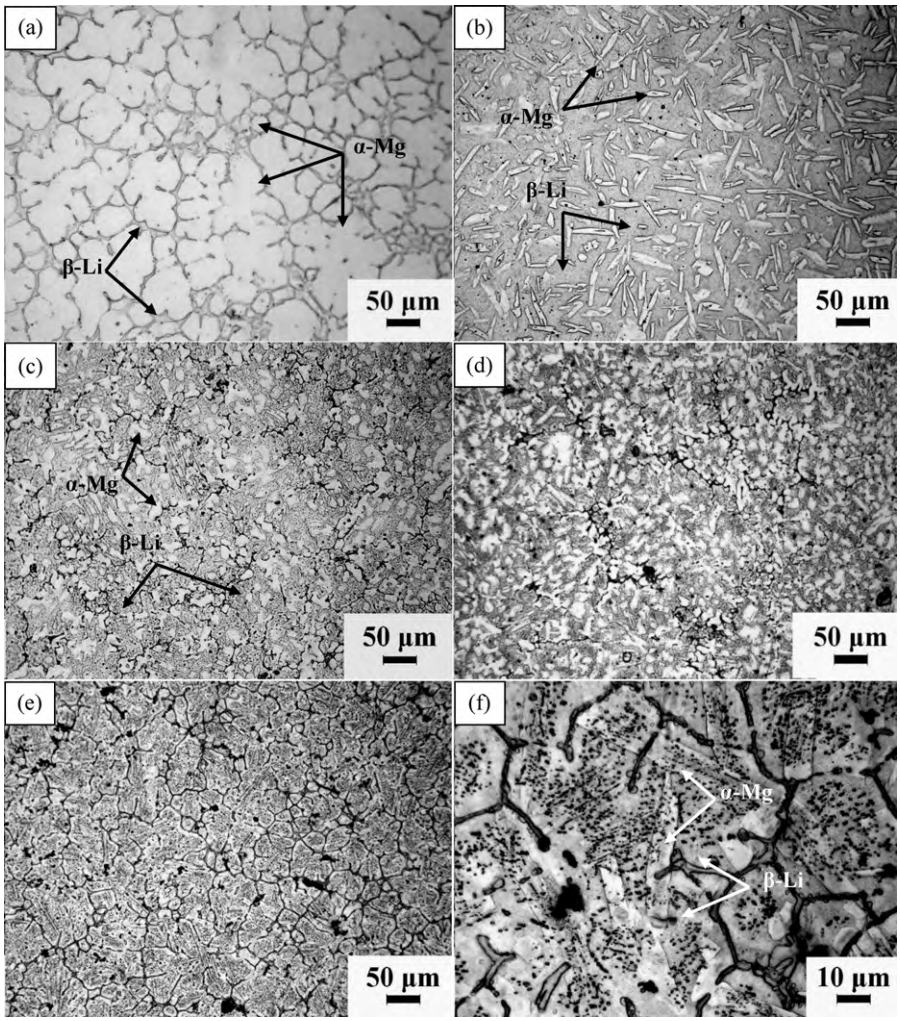

Fig. 3. Optical microscopy images of the as-cast Mg–7Li–(0–7)Y alloys: (a) Mg–7Li alloy, (b) Mg–7Li–1Y alloy, (c) Mg–7Li–3Y alloy, (d) Mg–7Li–5Y alloy, (e) Mg–7Li–7Y alloy (200×) and (f) Mg–7Li–7Y alloy (1000×).

solid solubility of Y. The absence of $Mg_{24}Y_5$ in the XRD pattern of Mg–7Li–3Y alloy is presumably due to its little amount in this alloy. The white round dots in Mg–7Li–1Y alloy are composed of Mg, Y and O elements. The existence of oxygen implies the oxidation of the alloy.

The Mg:Y weight ratio in the β matrix of the Y-containing alloys is 99.61:0.39, which is also listed in Table 2. Because the Mg proportion of Li-based β matrix in the duplex Mg–Li alloys is no more than 89.3 wt.% [2], the Y fraction in the β matrix of Mg–7Li–(1–7)Y alloys is calculated to be about 0.35 wt.%. In other words, the solubility of Y, as a RE element, in the Li-based β matrix is fairly low, and Y element is difficult to dissolve in the Li-based phase. It was also reported that the Gd element has a low solubility in Li [20].

The formation of the precipitates in the Y-containing alloys is attributed to the change of Y solubility from the liquid alloy melts to solid alloys. According to the Mg–Y binary diagram [18], Y atoms are completely solved in the liquid alloy melts. As the solidification begins, there is a large decrease of Y solubility from the melts to α and β phases in the alloys, and this decrease leads to the abundance of Y atoms and results in the precipitates of Y element. It has been reported when Li atoms deposit onto the Mg–9Y alloy cathode of the electrolysis unit, Li diffuses into the cathode and leads to a Y-enriched α-Mg phase in the Mg–9Y alloy [21]. It is believed to be mainly ascribed to the low solubility of Y in the β-Li matrix [21]. In Mg–7Li–(1–5)Y alloys, as the Y content increases from 1 wt.% to 5 wt.%, the abundant amount of Y atoms also increases. This consequently leads to the increasing amount of precipitates in the β phase. Meanwhile, the Y-enriched α-Mg phase is also formed in the α-Mg matrix of Mg–7Li–7Y alloy because of the high Y content in this alloy.

The differences between the compositions of precipitates can be explained in terms of different forming procedures. The solidification is assumed to begin near the eutectic temperature of Mg–Li binary system (588 °C) [2], which is higher than that of Mg–Y binary system (566 °C) [18]. After the solidification of α-Mg phase, the solid β phase appears. The decrease of Y solubility makes the solid β phase over-saturated by Y atoms and leads to a large amount of Y-enriched α-Mg phase in the β matrix and along the edge of α-Mg phase. For Mg–7Li–7Y alloy, at the beginning of solidification, α-Mg phase is already over-saturated by Y element, and, therefore, the Y-enriched α-Mg phase is formed in both α-Mg and β-Li matrixes.

Besides the Y element in the Y-enriched α-Mg phase, there still remain some abundant Y atoms in Mg–7Li–(3–7)Y alloys. As the temperature decreases to 566 °C, these Y atoms form the eutecticum of $Mg_{24}Y_5$ and the α-Mg solution with the maximal solid solubility of Y. The increasing amount of the eutecticum phase is ascribed to the increase of the abundant Y atoms in Mg–7Li–(3–7)Y alloys. Because the decomposition temperature of

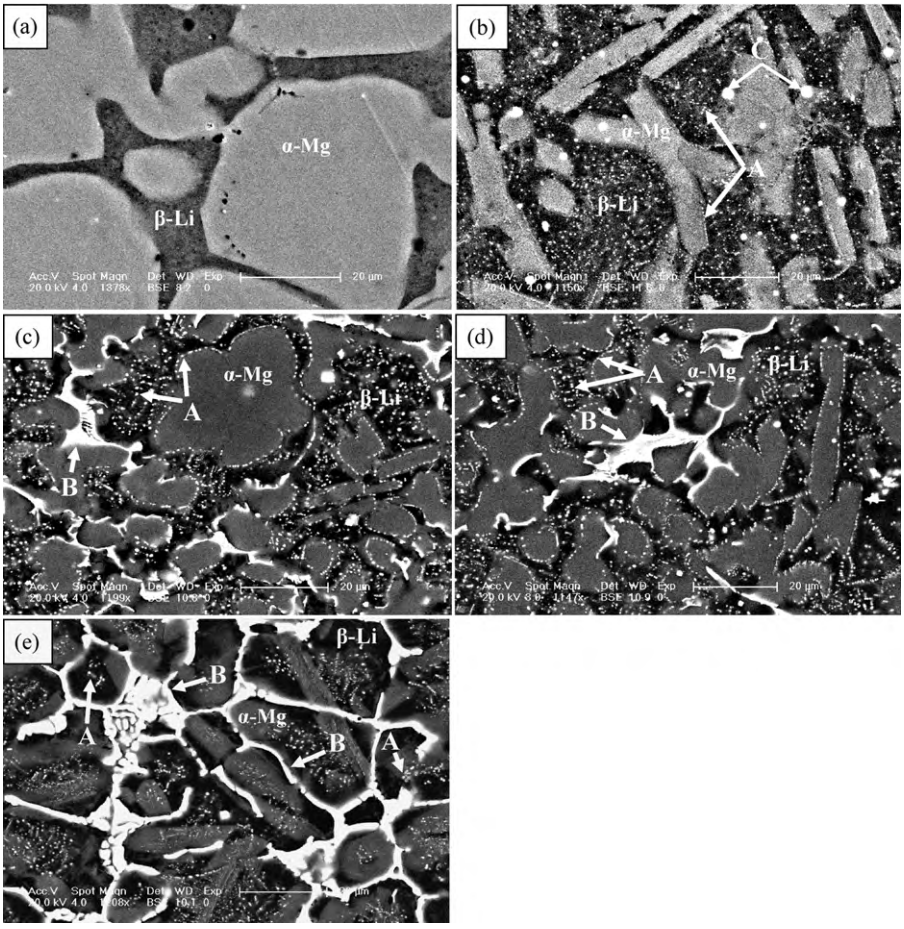

Fig. 4. SEM images of the as-cast Mg–7Li–(0–7)Y alloys: (a) Mg–7Li alloy, (b) Mg–7Li–1Y alloy, (c) Mg–7Li–3Y alloy, (d) Mg–7Li–5Y alloy, and (e) Mg–7Li–7Y alloy (The Y-enriched α-Mg phase (A), eutecticum (B) and oxidation (C)).

$Mg_{24}Y_5$ (605 °C) is higher than 566 °C, $Mg_{24}Y_5$ is stable after being formed.

3.2. Mechanical properties of as-cast alloys

The mechanical properties of the as-cast Mg–7Li–(0–7)Y alloys are plotted in Fig. 5. Both ultimate tensile strength (UTS) and yield strength (YS) of the Y-containing alloys are higher than those of Mg–7Li alloy. When Y content is lower than 5 wt.%, the strength of the alloys increases when increasing the Y content. The highest ultimate tensile strength, possessed by Mg–7Li–5Y alloy, is 41% higher than that of Mg–7Li alloy. The highest yield strength of Mg–7Li–7Y alloy is nearly as twice as that of Mg–7Li alloy. The ductility of the alloys is increased with the Y addition of no more than 3 wt.%, and further addition of Y element leads to a sharp decrease of the elongation. Mg–7Li–1Y alloy possesses the highest elongation of 33%. Mg–7Li–3Y alloy shows a favorable combination of the strength and elongation, and its ultimate tensile strength, yield strength and elongation are 160 MPa, 144 MPa and 20%, respectively.

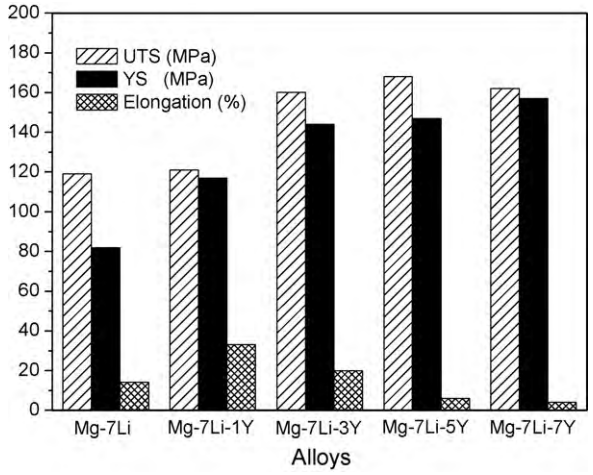

Fig. 5. Mechanical properties of the as-cast Mg–7Li–(0–7)Y alloys (tensile rate = 3.3×10^{-4} s^{-1}).

Fig. 6 plots the HV and HB of the as-cast Mg–7Li–(0–7)Y alloys, and also the HV of α and β phases in these alloys. The hardness of the Y-containing alloys, as well as the hardness of α and β phases, is higher than that of Mg–7Li alloy. Mg–7Li–3Y alloy possesses the highest HV hardness of α and β phases, and the peak HB hardness also appears in Mg–7Li–3Y alloy, the HV of Mg–7Li–5Y alloy is almost the same as that of Mg–7Li–3Y alloy. The hardness improvement of the Y-containing alloys is similar to the strength enhancement of these alloys.

It is noted that the HV of α phase increases with the increasing addition of Y element in Mg–7Li–(1–3)Y alloys. This is mainly attributed to the Y atoms solutionized in this phase since there is no precipitate in the α phase of the alloys (as seen in Fig. 4). The HV of β phase increases gradually with the increasing amount of Y in Mg–7Li–(1–3)Y alloys. It is ascribed to the precipitates in the β matrix, because the Y content in the β matrix is too low to introduce evident solid-solution strengthening effect. In addition, it can also be observed that the HV of Mg–7Li–5Y alloy is higher than those

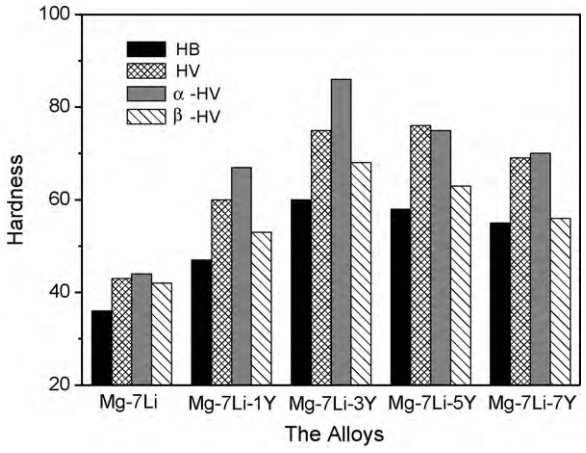

Fig. 6. Hardness of the as-cast Mg–7Li–(0–7)Y alloys.

of both α and β phases in this alloy, which implies that the alloy is also strengthened by some other mechanisms besides the Y atoms in the α phase and precipitates in the β matrix. This situation can be explained by the Y-enriched α-Mg phase arranging along the edge of α-Mg grains. These particles present to be beneficial to the HV enhancement of the Y-containing alloys.

3.3. Mechanical properties of heat-treated alloys

The eutectic temperature, which is also the melting temperature (T_m), of Mg–Li binary system is 588 °C (861 K) [2], and that of Mg–Y binary system is 566 °C (839 K) [18]. The solutionizing temperatures for Mg–Li and Mg–Y binary systems are calculated, by $0.75T_m$, to be 373 °C (646 K) and 356 °C (629 K), respectively. In order to enable the Li-based phase to be fully solutionized as the other phases, the solutionizing heat treatment of Mg–7Li–(1–7)Y alloys begins at of 375 °C and 400 °C. The HV of Mg–7Li–(1–7)Y alloys solutionized for 3 h at 375 °C and 400 °C is plotted in Fig. 7. The Y-containing alloys show a hardness descent after being solutionized. As seen in Fig. 7, the HV of Mg–7Li–7Y alloy decreases when the temperature increases from 375 °C to 400 °C. Therefore, the solutionizing heat treatment is enhanced to 425 °C and 450 °C. Fig. 7 also shows the HV of Mg–7Li–(1–7)Y alloys solutionized for 3 h at 425 °C and 450 °C. At 425 °C, the hardness of Mg–7Li–3Y alloy presents a rapid decrease, and Mg–7Li–5Y alloy also gets a descent in HV. As the temperature increases to 450 °C, the HV of Mg–7Li–3Y alloy shows a distinct increase, and the HV values of Mg–7Li–(5–7)Y alloys are almost the same as those of 425 °C. It seems that Mg–7Li–1Y alloy is fully solutionized at 400 °C and Mg–7Li–(3–7)Y alloy can be sufficiently solutionized at 425 °C.

In Mg–Li system alloys, high temperature leads to high loss of Li at surfaces of the ingots and samples and also offers the potential of the oxidation of the alloys. As the ductility is also concerned, a relatively low solutionizing temperature of 400 °C is applied to enhance the elongation of the as-cast Y-containing alloys, especially Mg–7Li–1Y alloy, which possesses the highest elongation. Mg–7Li–1Y and Mg–7Li–7Y alloys are selected to be T6 heat-treated with a subsequent aging treatment at 100 °C after being T4 heat-treated at 400 °C for 3 h. Fig. 8 plots the HV of Mg–7Li–1Y and Mg–7Li–7Y alloys aged for 1–72 h. Mg–7Li–1Y and Mg–7Li–7Y alloys show small HV variations near the value of 53 and 63, respectively. After being aged for 12 h, the HV of Mg–7Li–1Y alloy increases to the peak value of 56. Mg–7Li–7Y alloy seems not to be fully solutionized at 400 °C for 3 h, since there is a HV decrease in the initial period of aging. The peak HV of Mg–7Li–7Y alloy appears at the aging time of both 12 h and 24 h with the value of 66.

Fig. 9 shows the tensile properties of T4 and T6 heat-treated Mg–7Li–1Y and Mg–7Li–7Y alloys. The strength of the heat-treated alloy is lower than that of the corresponding as-cast alloy. The ultimate tensile strength and yield strength of T4 heat-treated

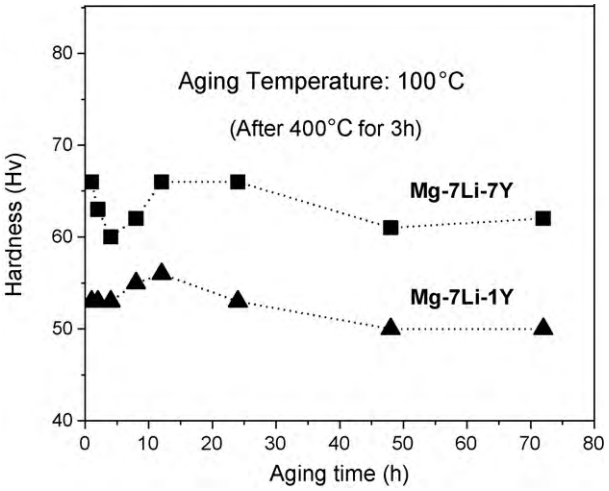

Fig. 8. HV of Mg–7Li–1Y and Mg–7Li–7Y alloys aged at 100 °C after solutionized at 400 °C for 3 h.

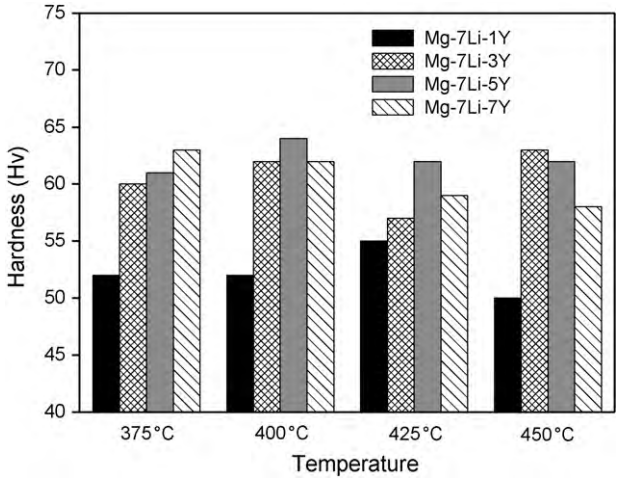

Fig. 7. HV of Mg–7Li–(1–7)Y alloys solutionized for 3 h.

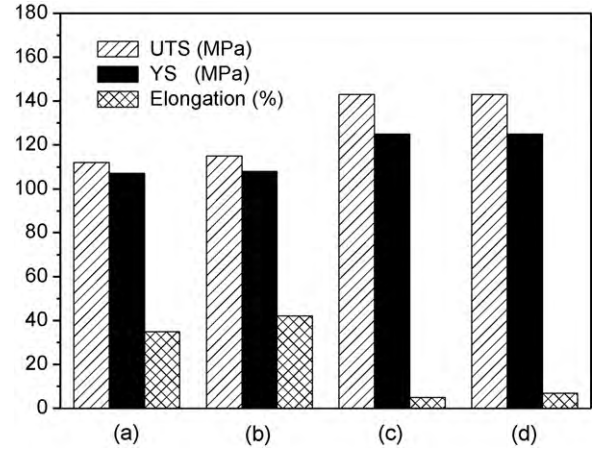

Fig. 9. Mechanical properties of (a) T4 and (b) T6 heat-treated Mg–7Li–1Y alloy, and (c) T4 and (d) T6 heat-treated Mg–7Li–7Y alloys (tensile rate = 3.3×10^{-4} s^{-1}).

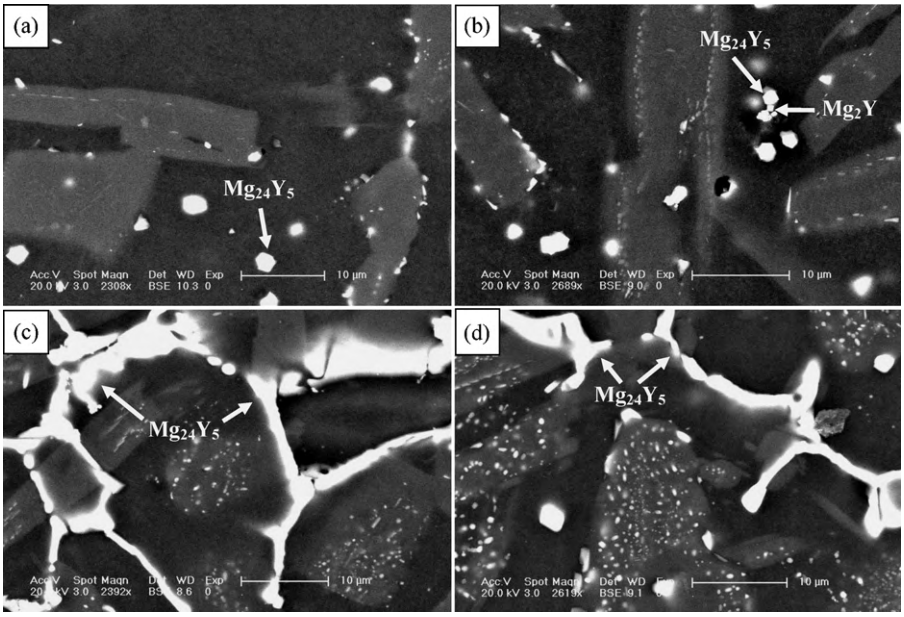

Fig. 10. SEM images of (a) T4 and (b) T6 heat-treated Mg–7Li–1Y alloy, and (c) T4 and (d) T6 heat-treated Mg–7Li–7Y alloys.

Mg–7Li–1Y alloy are almost the same as those of T6 state, which is consistent with the HV results in Figs. 7 and 8. The elongation of the heat-treated Mg–7Li–1Y alloy is higher than that of the as-cast alloy. These situations can also be seen in Mg–7Li–7Y alloy.

Fig. 10 illustrates the microstructures of Mg–7Li–1Y and Mg–7Li–7Y alloys after T4 and T6 heat treatments. The microstructures of T4 heat-treated Mg–7Li–1Y and Mg–7Li–7Y alloys are nearly the same as those of the corresponding T6 heat-treated alloys. The Y-enriched α-Mg phase shows a decrease in amount and nearly disappears in the β phase of the heat-treated alloys. There exist some hexagonal and cubic phases in the β phase of the heat-treated Mg–7Li–1Y alloy. XRD patterns of the heat-treated Mg–7Li–1Y and Mg–7Li–7Y alloys are shown in Fig. 11. It is indicated that Mg_2Y and $Mg_{24}Y_5$ appear in the heat-treated Mg–7Li–1Y alloy. According to the compositions in Table 3, the newly formed $Mg_{24}Y_5$ is recognized as the hexagonal phase, and Mg_2Y is concluded to be the cubic one.

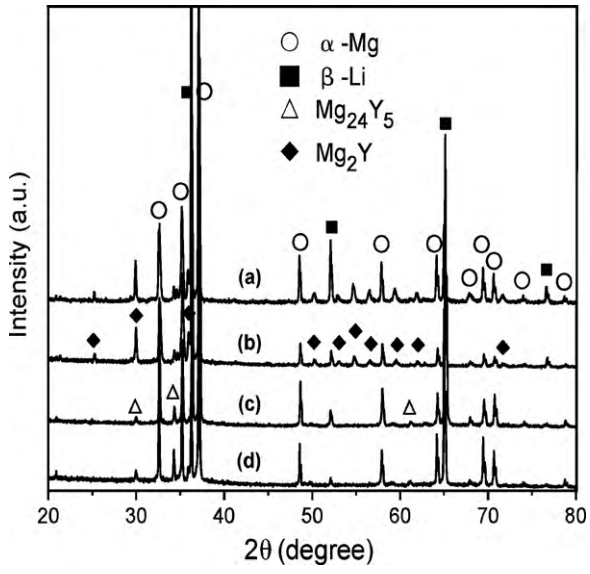

Fig. 11. XRD patterns of (a) T4 and (b) T6 heat-treated Mg–7Li–1Y alloy, and (c) T4 and (d) T6 heat-treated Mg–7Li–7Y alloys.

Table 3
The compositions of the phases in the heat-treated Mg–7Li–1Y alloy determined by EDS: the cubic phase (a) and hexagonal phase (b).

	(a)		(b)	
	Mg	Y	Mg	Y
wt.%	33.34	66.66	60.10	39.9
at.%	64.63	35.37	84.63	15.37
Mg:Y (atomic ratio)	1.83:1		5.51:1	

The strength decrease of the heat-treated alloys is resulted from the decrease of the amount of precipitates in the Y-containing alloys. The increase of elongation is also attributed to the decrease of the Y-enriched α-Mg phase in the β phase. The consistence of the hardness and mechanical properties of the heat-treated Y-containing alloys can be explained by the consistence of the microstructures.

4. Conclusions

The α-Mg and β-Li phases exist in all Mg–7Li–*x*Y (*x* = 0–7 wt.%) alloys. Y element has a low solubility in the Li-based β phase. Y addition refines the α-Mg phase, and introduces two kinds of precipitates to Mg–7Li–(1–7)Y alloys. One kind of precipitates is the particle-like Y-enriched α-Mg phase, and the other is the lamellar and branch-like eutecticum phase of $Mg_{24}Y_5$ and the α-Mg solution with the maximal solid solubility of Y element.

The strength is enhanced by both the solid-solution strengthening effect of α phase and precipitate hardening effect introduced by Y element. The elongation is improved with the Y addition no more than 3 wt.%. In the as-cast alloys, Mg–7Li–1Y alloy possesses the highest elongation of 33%, and Mg–7Li–3Y alloy exhibits an optimum combination of strength and elongation. For Mg–7Li–3Y alloy, the ultimate tensile strength, yield strength and elongation are 160 MPa, 144 MPa and 22%, respectively. Y addition more than 3 wt.% shows little further enhancement to the strength but decreases the ductility of the alloys rapidly.

After the solutionizing treatments for 3 h at the temperatures from 375 °C to 450 °C, some of the Y-enriched α-Mg phase dissolves,

and the strength of the Y-containing alloys is decreased. After solutionized at 400 °C for 3 h, the subsequent aging heat treatment at 100 °C introduces little effect on the microstructure and strength of Mg–7Li–1Y and Mg–7Li–7Y alloys.

Acknowledgments

This work is financially supported by the Foundation for Innovative Research Groups of the National Natural Science Foundation (20921002) and the Science and Technology Supporting Project of Changchun City (2007KZ05). The authors would also show their thanks to Dr. Wang Jianli, Dr. Peng Qiuming and Mr. Xiao Wenlong for their beneficial discussions.

References

[1] F.E. Hauser, P.R. Landon, J.E. Dorn, Trans. ASM 50 (1958) 856–881.
[2] W. Gąsior, Z. Moser, W. Zakulski, G. Schwitzgfbel, Metall. Mater. Trans. A 27 (1996) 2419–2428.
[3] R.J. Jackson, P.D. Frost, NASA SP-5068, Washington DC, 1967.
[4] C.P. Liang, H.R. Gong, J. Alloys Compd. 489 (2010) 130–135.
[5] B. Jiang, D. Qiu, M.X. Zhang, P.D. Ding, L. Gao, J. Alloys Compd. 492 (2010) 95–98.
[6] S. González, D.V. Louzguine-Luzgin, J.H. Perepezko, A. Inoue, J. Alloys Compd. (2010), doi:10.1016/j.jallcom.2010.02.141.
[7] J.H. Jackson, P.D. Frost, A.C. Loonam, L.W. Eastwood, C.H. Lorig, JOM 2 (1949) 149–168.
[8] G.S. Foerster, H.A. Diehl, NASA Contract: NAS5-10398, Maryland, 1968.
[9] O. Tanno, K. Ohuchi, K. Matuzawa, S. Kamado, Y. Kojima, J. Jpn. Inst. Light Met. 42 (1992) 3–9.
[10] W.R.D. Jones, J. Inst. Met. 84 (1955/1956) 364-378.
[11] K. Ohuchi, S. Iwasawa, S. Kamado, Y. Kojima, R. Ninomiya, J. Jpn. Inst. Light Met. 42 (1992) 446–452.
[12] R. Ninomiya, K. Miyake, J. Jpn. Inst. Light Met. 51 (2001) 509–513.
[13] H. Takuda, S. Kikuchi, N. Yoshida, H. Okahara, Mater. Trans. 44 (2003) 2266–2270.
[14] R.K. Wyss, in: H. Paris, W.H. Hunt (Eds.), Advances in Mg Alloys and Composites, 1988, pp. 25–40, Pennsylvania.
[15] L. Zhao, P. Zhao, Heat Treat. Met. 33 (8) (2008) 37–40.
[16] P. Metenier, G. González-Doncel, O.A. Ruano, J. Wolfenstine, O.D. Sherby, Mater. Sci. Eng. A 125 (1990) 195–202.
[17] M. Furui, H. Kitamura, H. Anada, T.G. Langdon, Acta Mater. 55 (2007) 1083–1091.
[18] A.A. Nayeb-Hashemi, J.B. Clark, Phase Diagrams of Binary Magnesium Alloys, ASM, 1988.
[19] Y.W. Kim, D.H. Kim, H.I. Lee, C.P. Hong, Scripta Mater. 38 (1998) 923–929.
[20] D.G. Kevorkov, J. Gröbner, R. Schmid-Fetzer, V.V. Pavlyuk, G.S. Dmytriv, O.I. Bodak, J. Phase Eqilib. (Section I) 22 (2001) 34–42.
[21] H.W. Dong, L.D. Wang, Y.M. Wu, L.M. Wang, Metall. Mater. Trans. B 40 (2009) 779–784.